Quantitative Spectroscopic Diffuse Optical Tomography of the Breast Guided by Imperfect A Priori Structural Information

Gregory Boverman[1]§, Eric L Miller[1], Ang Li[2], Quan Zhang[3], Tina Chaves[3], Dana H Brooks[1], and David A Boas[3]

[1] Department of Electrical and Computer Engineering, Northeastern University, 302 Stearns Hall, Boston, MA 02115

[2] Martinos Center for Biomedical Imaging, Massachusetts General Hospital, 149 Thirteenth Street, Suite 2301, Charlestown, MA 02129

[3] Beckman Laser Institute, University of California, Irvine, 1002 Health Sciences Road, East Irvine, CA 92612

Abstract. Spectroscopic Diffuse Optical Tomography (DOT) can directly image the concentrations of physiologically significant chromophores in the body. This information may be of importance in characterizing breast tumors and distinguishing them from benign structures. This paper studies the accuracy with which lesions can be characterized given a physiologically realistic situation in which the background architecture of the breast is heterogeneous yet highly structured. Specifically, in simulation studies, we assume that the breast is segmented into distinct glandular and adipose regions. Imaging with a high-resolution imaging modality, such as Magnetic Resonance Imaging, in conjunction with a segmentation by a clinical expert, allows the glandular/adipose boundary to be determined. We then apply a two-step approach in which the background chromophore concentrations of each region are estimated in a nonlinear fashion, and a more localized lesion is subsequently estimated using a linear perturbational approach. In addition, we examine the consequences which errors in the breast segmentation have on estimating both the background and inhomogeneity chromophore concentrations.

§ To whom correspondence should be addressed (gboverma@ece.neu.edu)

1. Introduction

Near infrared (NIR) light is beginning to show great promise as a means of noninvasively probing tissue. NIR light is able to penetrate several centimeters through the body, and the differences between the spectra of Oxy-Hemoglobin (HbO) and Deoxy-Hemoglobin (HbR) make spatially localized functional imaging of the body's hemodynamics possible. In addition, H_2O and lipids have spectral peaks in this region, in principle making possible the imaging of these chromophores as well (Cubbedu et al. 1999). In contrast to imaging modalities such as X-rays and MRI, NIR imaging can be accomplished using non-ionizing radiation and low-cost, potentially portable, electronic components. However, imaging the body's chromophore distributions, which we will refer to here as Diffuse Optical Tomography (DOT), is made quite difficult by the highly turbid nature of NIR light propagation within tissue, with photons generally experiencing many scattering events in their paths.

Near-infrared spectroscopy and imaging has been applied to a number of biomedical applications (Boas, Brooks, Miller, Dimarzio, Kilmer, Gaudette & Zhang 2001), including functional brain imaging (Chance et al. 1998, Franceschini et al. 2000), monitoring of strokes (Vernieri et al. 1999), neonatal hymodynamics (Hebden et al. 2002), and the imaging of breast tumors (Dehghani et al. 2003, Franceschini et al. 1997, Grosenick et al. 1999). In the domain of breast imaging, DOT, by virtue of its ability to directly measure physiologically significant parameters, may prove to be a valuable adjunct to X-ray mammography, a technology that is currently prone to a high rate of false-positive tumor detections (Elmore et al. 1998) (Banks et al. 2004) (Fletcher & Elmore 2003).

In DOT, tissue is illuminated by NIR light sequentially at a number of source locations, generally coupled to the body by means of fiber-optic components. In frequency-domain DOT, the light is RF modulated, producing Diffuse Photon Density Waves (DPDW's) within the body. The resulting attenuation and phase shifts are measured at a number of detector positions, with Photomultiplier Tubes (PMT's), Avalanche Photodiodes (APD's), or Charged-Coupled Devices (CCD's) used for light detection. The significant problems of sensor calibration are described elsewhere (Boas, Gaudette & Arridge 2001, Oh et al. 2002). The measured amplitude and phase shifts (with respect to a theoretically known background) are used to reconstruct the optical properties, specifically the absorption and reduced scattering coefficient, $\mu_a(\lambda)$ and $\mu_s'(\lambda)$, at a given wavelength of light, λ. This reconstruction is typically accomplished using either linearized methods, which make a number of assumptions with respect to inhomogeneity size and/or contrast, or through the use of nonlinear optimization approaches (i.e. gradient-descent or Newton-based), which can be very computionally costly.

Although DOT holds a great deal of promise for breast-cancer screening, it presents very difficult technical problems. The most significant limitations of DOT imaging are the smoothing and nonlinear properties of the light propagation model, the consequences of

which are the ill-posedness and nonlinearity of the inverse problem, respectively. This ill-posedness can be ameliorated by means of regularization, but this introduces the further difficulty of regularization operator and regularization parameter selection.

Early work in this field concentrated on reconstruction of the medium's optical properties for a given wavelength of light (Jiang et al. 1996, Jiang et al. 1997, Milstein et al. 2002). Recently, researchers have begun to combine measurements taken at a number of wavelengths, reconstructing an image at each wavelenth and using a least-squares fit in order to estimate the distribution of chromophoes within the body (McBride et al. 1999, Pogue et al. 2001).

Most recently, a method has been proposed to directly image the chromophore concentrations within the body (Gaudette et al. 1999, Hillman 2002, Li et al. 2004, Li et al. 2005) without first estimating the optical properties. Simulation results have shown a reduction in cross-talk and improvement in resolution made possible by this "direct" form of spectroscopic imaging as compared to the "indirect" approach previously reported in the literature.

The issue of the heterogeneity of breast tissue, with respect to tissue optical properties, has only recently begun to be examined. One study (Shah et al. 2004) directly examined this question, making use of NIR frequency-domain spectroscopy at seven wavelengths for 31 patients. Significant, reproducible, spatial heterogeneity was observed for hemoglobin concentration, H_2O concentration, and lipid concentration, with the degree of heterogeneity being somewhat age-dependent. As this research made use of spectroscopy rather than diffuse optical imaging, the question of how the heterogeneity within the breast is spatially distributed has not yet been clearly answered. A study (Cubbedu et al. 2000), making use of time-domain data, also found significant differences between measurements of total hemoglobin, oxygen saturation, and amounts of H_2O and lipids made at different points on the surface of the breast, as well as differences between reflectance and transmission measurements. Another study (Shah et al. 2001), making use of frequency-domain data for four wavelengths over a wide range of modulation frequencies, found variations in breast hemoglobin concentration, μ_s', and breast water content to be correlated with age. These variations were postulated to be a result of the breast's changing composition, and specifically with the atrophy of the glandular tissue as a woman ages. A larger study (Cerussi et al. 2001), using measurements at seven wavelengths, confirmed these results and found breast lipid content to be correlated to age as well. Two studies (Srinivasan et al. 2003, Durduran et al. 2002) investigating the bulk properties of the breast found a correlation between Body Mass Index (BMI) and total hemoglobin concentration. It therefore seems reasonable to postulate that there are significant optical differences between the glandular and adipose tissues present in the female breast, although this assumption has not been definitively validated by empirical investigations.

In this paper, we assume that the breast is composed of distinct glandular and adipose

regions with piecewise constant optical properties, and that the boundary between them can be determined by concurrent imaging with a higher spatial resolution imaging modality, such as X-ray imaging, ultrasound, or magnetic resonance imaging (MRI). The existence of these regions, whose size and properties vary as a woman ages and, most likely, at different points in the menstrual cycle, is clear from MRI scans, as in Fig. 1. In our simulations, we examine the effect on reconstruction quality of significant differences between glandular and adipose tissues in blood volume and in lipid concentration.

A number of papers have addressed the use of prior information in the solution of the inverse problem. Researchers (Pogue & Paulsen 1998) showed that hemodynamic imaging of a rat cranium could be improved by including anatomical information from a high-resolution MRI scan. Li (Li et al. 2003) examines the linear inverse problem with a spatial constraint, incorporating the spatial prior by means of a second regularization parameter in the region in which the anomaly is believed to reside. Simulation results showed that the suggested multiple regularization parameter selection algorithm is robust to incorrect prior information. Others (Hero et al. 1999) introduced an algorithm to make use of noisy information about the shape of a region's boundary in estimating the radionucleide uptake within the region. A number of studies (Huang et al. 2003, Brooksby et al. 2003) have combined NIR imaging with other modalities and have quantified the improvement in anomaly characterization, using measurements at a single wavelength, achieved by means of incorporating prior spatial information from coregistered MRI and ultrasound images. The use of prior spatial and spectroscopic prior information has been reported (Intes et al. 2004), as well as a Bayesian approach to the inclusion of *a priori* anatomical information (Guven et al. 2005).

Here, we study the importance of accurately modeling the background structure to localizing a tumor and characterizing its spectroscopic properties. To this end, information from other imaging modalities can be used to demarcate the boundary between the two tissues, and the estimation of the spectral properties of each tissue type is reduced to a low-dimensional nonlinear optimization problem. In a realistic imaging situation, our information about the breast structure is likely to be imperfect, due to a number of factors: noise in the underlying X-ray or MRI measurements and image artifacts in the reconstructions for these imaging modalities, segmentation errors, and errors in the simultaneous co-registration of several three-dimensional images.

In this work, we examine, both qualitatively and quantitatively, the sensitivity of the tumor spectroscopic reconstruction with respect to errors in our prior knowledge of the breast background structure. Four cases are explored: assuming that the breast is homogeneous, assuming a dilated glandular region, assuming an eroded glandular region, and knowledge of the true background structure. In the dilated and eroded cases, the estimated glandular segmentations are greater and smaller in volume, respectively, than the true glandular region, as shown in Fig. 2. Given our segmentation, we first estimate the overall chromophore concentrations of the two regions directly, using a Gauss-Newton optimization approach,

and then estimate the inhomogeneity using a linear, perturbational algorithm. Thus, errors in estimation of the tumor's spectroscopic properties will occur in two places: error in computing the mismatch between the expected and actually measured data, and error in the sensitivity matrices used in the linear perturbational model.

Our results qualitatively show that even incorrect information about the background structure is useful in quantifying tumor chromophore concentrations and in reducing imaging artifacts, particularly for perturbations in oxyhemoglobin and deoxy-homoglobin (HbR and HbO), which are assumed to be much greater than the differences in blood volume and oxygen saturation between the two tissue types. As we have assumed that glandular and adipose tissues differ more sharply in their lipid content, reconstruction of perturbations of the same order is more problematic. We also quantify the reconstruction error as a function of regularization parameter, both within and outside the tumor, for all four cases, assuming perturbations in individual chromophores within the tumor. We find that large errors in the estimation of one chromophore's perturbation tend to be relatively isolated within that chromophore's reconstruction.

2. Methods

2.1. Forward Modeling

In the simulations that follow, we make use of the diffusion approximation (Arridge 1999, Boas 1996): to model the steady-state intensity and phase distribution due to a modulated source, making use of a zero partial flux boundary condition (Aronson 1995, Haskell et al. 1994) to model the air-tissue interface:

$$\begin{cases} -\nabla \cdot D(\mathbf{r})\nabla\phi(\mathbf{r},\omega) + (\mu_a(\mathbf{r}) + \frac{j\omega}{v})\phi(\mathbf{r},\omega) = S_0(\mathbf{r},\omega) & \mathbf{r} \in \Omega \\ \frac{1}{2}R_\phi\,\phi(\mathbf{r}) - D(\mathbf{r})R_j\;\hat{n}\cdot\nabla\phi(\mathbf{r}) = 0 & \mathbf{r} \in \bar{\Omega}\backslash\Omega \end{cases} \tag{1}$$

where the diffusion coefficient, $D(\mathbf{r})$ is $\frac{1}{3\mu_s'(\mathbf{r})}$, $\mu_a(\mathbf{r})$ is the absorption coefficient, and $\mu_s'(\mathbf{r})$ is the reduced scattering coefficient. The photon fluence is $\phi(\mathbf{r},\omega)$, a function of position, $\mathbf{r}$, and modulation frequency, ω. The isotropic source intensity is $S_0(\mathbf{r},\omega)$, and v is the speed of light in tissue. The dependence of all the parameters on the wavelength, λ is implicit. The spatial extent of the diffusive region is Ω. The Fresnel boundary reflection coefficients for the photon density and current are R_ϕ and R_j, respectively, and $\hat{n}$ is the direction normal to the boundary.

In a typical DOT experiment, tissue is illuminated at M source positions, and, for each source, measurements are made at N detector positions. This procedure is repeated for a number of wavelengths. It is also possible to make use of a number of modulation frequencies, but we will assume that all experiments use a modulation frequency of 70 MHz. We further make the assumption that the absorption at each point in space is a linear combination of

C chromophores whose spectra have been experimentally determined (Li et al. 2005):

$$\mu_a(\mathbf{r}, \lambda) = \sum_{j=1}^{C} \epsilon_j(\lambda) c_j(\mathbf{r}) \tag{2}$$

where $\epsilon_j(\lambda)$ is the extinction coefficient of chromophore j for light of wavelength λ, and $c_j(\mathbf{r})$ is the chromophore concentration. Specifically, we assume that the absorption at each wavelength is due to the following four chromophores: oxy and deoxy-hemoglobin, H_2O, and lipids. Motivated by Mie scattering theory, the reduced scattering coefficient is modeled as follows:

$$\mu_s'(\mathbf{r}, \lambda) = a(\mathbf{r}) \lambda^{-b(\mathbf{r})} \tag{3}$$

where $a(\mathbf{r})$ represents the scattering amplitude and $b(\mathbf{r})$ is related to average particle size.

In our simulations, the following wavelengths of light have been used: 685, 750, 808, 830, 906, and 980 nm. The first four wavelengths are intended to quantify concentrations of HbR and HbO, and the last two are situated near peaks in the spectra for H_2O and lipids, and are intended to discern their concentrations. The discretized absorptions and concentrations have the following relationship:

$$\boldsymbol{\mu}_a = \mathbf{E}\mathbf{c} \tag{4}$$

where and $\boldsymbol{\mu}_a$, $\mathbf{c}$ are stacked vectors of absorption and concentration values for each voxel: $\boldsymbol{\mu}_a = \begin{bmatrix} \boldsymbol{\mu}_a(685) & \boldsymbol{\mu}_a(750) & \boldsymbol{\mu}_a(808) & \boldsymbol{\mu}_a(830) & \boldsymbol{\mu}_a(906) & \boldsymbol{\mu}_a(980) \end{bmatrix}^T$, $\mathbf{c} = \begin{bmatrix} \mathbf{c}_{\mathrm{HbO}} & \mathbf{c}_{\mathrm{HbR}} & \mathbf{c}_{\mathrm{H_2O}} & \mathbf{c}_{\mathrm{L}} \end{bmatrix}^T$. The matrix $\mathbf{E}$ transforms an image in terms of chromophore concentrations into an image in terms of absorptions at each wavelength.

2.2. Inverse Problem Solution

As the inverse problem for DOT is generally severely underdetermined and ill-posed, some form of regularization, or prior information, is necessary in order to stabilize the inversion procedure. Thus, the inverse problem is often reduced to minimization of the following functional (Arridge 1999, Milstein et al. 2002, Li et al. 2003):

$$L = \arg\min_{\mathbf{c},\mathbf{a}} ||\mathbf{y} - \mathbf{h}(\mathbf{c}, \mathbf{a})||^2_{\boldsymbol{\Sigma}_n^{-1}} + r(||\mathbf{c}||_2^2 + ||\mathbf{a}||_2^2) \tag{5}$$

where $\boldsymbol{\Sigma}_n$ is the measurement noise covariance matrix (assumed to be diagonal in this paper), $\mathbf{y} = \begin{bmatrix} \mathbf{y}^{685} & \mathbf{y}^{750} & \mathbf{y}^{808} & \mathbf{y}^{830} & \mathbf{y}^{906} & \mathbf{y}^{980} \end{bmatrix}^T$. and $\mathbf{h} = \begin{bmatrix} \mathbf{h}^{685} & \mathbf{h}^{750} & \mathbf{h}^{808} & \mathbf{h}^{830} & \mathbf{h}^{906} & \mathbf{h}^{980} \end{bmatrix}^T$, $\mathbf{h}^{\lambda}$ being the hypothesized measurements at wavelength λ, which can be generated by means of the finite-difference method. The regularization parameter is denoted by r. We note that, in this work, we are making use of an identity regularization functional.

The adjoint method (Arridge 1999, Arridge 1995) can be used to compute, with fairly low computional cost, a first-order linear perturbational approximation for the change in the model solution, $\mathbf{h}$, with respect to changes in each voxel's chromophore concentrations and scattering amplitude relative to a known background:

$$\mathbf{h} \approx \mathbf{h}_0(\mathbf{c}_0, \mathbf{a}_0) + \mathbf{J}(\mathbf{c}_0, \mathbf{a}_0)\mathbf{p} \tag{6}$$

where

$$\mathbf{J} = \left[\text{ block diag}(\mathbf{J}_{\mu_a}^{685}\, \mathbf{J}_{\mu_a}^{750}\, \mathbf{J}_{\mu_a}^{808}\, \mathbf{J}_{\mu_a}^{830}\, \mathbf{J}_{\mu_a}^{906}\, \mathbf{J}_{\mu_a}^{980})\, \mathbf{E} \quad | \quad \mathbf{J}_a \right] \tag{7}$$

and

$$\mathbf{p} = \begin{bmatrix} \mathbf{c}_p \\ \mathbf{a}_p \end{bmatrix} \tag{8}$$

with $\mathbf{c}_p = \left[\begin{array}{cccc} \mathbf{c}_{p,\mathrm{HbO}} & \mathbf{c}_{p,\mathrm{HbR}} & \mathbf{c}_{p,\mathrm{H_2O}} & \mathbf{c}_{p,\mathrm{L}} \end{array} \right]$ being the vector of concentration perturbations, and $\mathbf{a}_p$ being the vector of perturbations in scattering amplitude. The vector $\mathbf{h}_0(\mathbf{c}_0, \mathbf{a}_0)$ is the *incident field*, which is dependent on an assumed background chromophore distrubution $\mathbf{c}_0$ and the background scattering amplitude distribution $\mathbf{a}_0$. The Jacobian matrix at wavelength λ with respect to absorption perturbations is $\mathbf{J}_{\mu_a}^{\lambda}(\mathbf{c}_0, \mathbf{a}_0)$, where the dependence on $\mathbf{c}_0$ and $\mathbf{a}_0$ will be assumed to be implicit, and the Jacobian matrix with respect to scattering amplitude is:

$$\mathbf{J}_a = \left[\begin{array}{cccccc} (\mathbf{J}_a^{685})^T & (\mathbf{J}_a^{750})^T & (\mathbf{J}_a^{808})^T & (\mathbf{J}_a^{830})^T & (\mathbf{J}_a^{906})^T & (\mathbf{J}_a^{980})^T \end{array} \right]^T \tag{9}$$

In order to simplify the exposition of our simulations, we assume in our simulations that all tissues have the same scattering amplitude. The least-squares solution to the linear inverse problem is then:

$$\hat{\mathbf{p}} = \mathbf{J}^T \mathbf{\Sigma}_n^{-\frac{1}{2}} (\mathbf{\Sigma}_n^{-\frac{1}{2}} \mathbf{J}\mathbf{J}^T \mathbf{\Sigma}_n^{-\frac{1}{2}} + r\mathbf{I})^{-1} \mathbf{\Sigma}_n^{-\frac{1}{2}} (\mathbf{y} - \mathbf{h}_0(\mathbf{c}_0, \mathbf{a}_0)) \tag{10}$$

In Eq. 10, we note than an error in our knowledge of the background concentrations can cause a systematic reconstruction error, by introducing an error in our estimate of the incident field, $\mathbf{h}_0(\mathbf{c}_0, \mathbf{a}_0)$, and by causing inaccuracies in the Jacobian, $\mathbf{J}$. It is these systematic errors that are analyzed in the simulation results that follow.

The direct spectral reconstruction approach to the inverse problem does impose an additional computational cost compared to more traditional processing schemes. Rather than solving for the absorption and scattering perturbations at each wavelength independently, we solve for all chromophore concentrations simultaneously, making use of measurements at all wavelengths. In the case of an identity regularization function and our particular configuration of sources and detectors, the solution is still computationally feasible with non-specialized computing hardware, and, if a more complex regularization function is employed, iterative methods, such as the LSQR algorithm (Paige & Saunders 1982), may be employed.

In this paper, we make use of the Generalized Cross-Validation (Golub et al. 1979, Golub & von Matt 1997) approach to regularization parameter selection, which is based on the Bayesian criterion of minimizing expected reconstruction error.

2.3. Estimation of background chromophore concentrations

Before the linear inverse problem can be solved, we must first estimate the *incident field*, $\mathbf{h}_0(\mathbf{c}_0, \mathbf{a}_0)$, in Eq. 10. Here, we assume that the breast is piecewise constant, with distinct glandular and adipose regions, and we must estimate the chromophore concentrations in these regions. We solve this optimization problem using the Gauss-Newton method, solving for the parameter vector $\mathbf{g} = \begin{bmatrix} \mathbf{g}_{1,HbR} & \mathbf{g}_{1,HbO} & \mathbf{g}_{1,H_2O} & \mathbf{g}_{1,L} & \mathbf{g}_{1,a} & \mathbf{g}_{2,HbR} & \mathbf{g}_{2,HbO} & \mathbf{g}_{2,H_2O} & \mathbf{g}_{2,L} & \mathbf{g}_{2,a} \end{bmatrix}^T$, where the adipose and glandular regions are labeled region 1 and region 2, respectively.

Now, we define the following indicator vectors, assuming a lexicographic ordering of the breast voxels in the forward problem:

$$(\mathbf{i}_j)_k = \begin{cases} 1, & \text{voxel k is in region j} \\ 0, & \text{voxel k is not in region j} \end{cases} \tag{11}$$

The Jacobian with respect to changes in background chromophore concentrations is computed as follows:

$$\mathbf{J_g} = \mathbf{J} \begin{bmatrix} \mathbf{i}_1 & \mathbf{0} & \mathbf{0} & \mathbf{0} & \mathbf{0} & \mathbf{i}_2 & \mathbf{0} & \mathbf{0} & \mathbf{0} & \mathbf{0} \\ \mathbf{0} & \mathbf{i}_1 & \mathbf{0} & \mathbf{0} & \mathbf{0} & \mathbf{0} & \mathbf{i}_2 & \mathbf{0} & \mathbf{0} & \mathbf{0} \\ \mathbf{0} & \mathbf{0} & \mathbf{i}_1 & \mathbf{0} & \mathbf{0} & \mathbf{0} & \mathbf{0} & \mathbf{i}_2 & \mathbf{0} & \mathbf{0} \\ \mathbf{0} & \mathbf{0} & \mathbf{0} & \mathbf{i}_1 & \mathbf{0} & \mathbf{0} & \mathbf{0} & \mathbf{0} & \mathbf{i}_2 & \mathbf{0} \\ \mathbf{0} & \mathbf{0} & \mathbf{0} & \mathbf{0} & \mathbf{i}_1 & \mathbf{0} & \mathbf{0} & \mathbf{0} & \mathbf{0} & \mathbf{i}_2 \end{bmatrix} \tag{12}$$

where $\mathbf{J}$ is the Jacobian with respect to voxel-wise changes in concentration and scattering amplitude.

Estimation of the parameter vector, $\mathbf{g}$, then proceeds by means of the Gauss-Newton algorithm, with a cubic line search.

2.4. Reconstruction Error Analysis

In this section, we analyze the image reconstruction error in the case of Gaussian noise, decomposing it into deterministic and stochastic components. Firstly, we assume that $\mathbf{y} = \mathbf{y}_m + \mathbf{n}$, where $\mathbf{y}_m$ is known and $\mathbf{n}$ is a zero-mean vector of Gaussian noise, with covariance matrix $\mathbf{\Sigma}_n$. For the sake of clarity, we assume in the analysis that follows that $\mathbf{h}_0$, $\mathbf{n}$, $\mathbf{J}$, and $\mathbf{y}$ have been pre-multiplied by $\mathbf{\Sigma}_n^{1/2}$.

The expected mean-squared reconstruction error for a given regularization parameter can be written as follows:

$$\mathbf{C} = E|| \mathbf{M}(\mathbf{c}_0 + \mathbf{p}) - \mathbf{M}(\hat{\mathbf{c}}_0 + \mathbf{J}^T(\mathbf{J}\mathbf{J}^T + r\mathbf{I})^{-1}(\mathbf{y}_m + \mathbf{n} - \mathbf{h}_0))||_2^2 \tag{13}$$

where $\mathbf{c}_0$ is the true background, $\mathbf{p}$ is the true perturbation, $\hat{\mathbf{c}}_0$ is the estimated background, and $\mathbf{M}$ is a selection matrix, focusing on a particular region of interest.

Assuming that the noise is statistically uncorrelated with $\mathbf{c}_0$, $\mathbf{p}$, $\hat{\mathbf{c}}_0$, $\mathbf{y}_m$, and $\mathbf{y}_0$, we can show that:

$$\mathbf{C} = \mathbf{C}_{\text{bias}} + \mathbf{C}_{\text{variance}} \tag{14}$$

where:

$$\mathbf{C}_{\text{bias}} = ||\,\mathbf{M}(\mathbf{c}_0 + \mathbf{p}) - \mathbf{M}(\hat{\mathbf{c}}_0 + \mathbf{J}^T(\mathbf{J}\mathbf{J}^T + r\mathbf{I})^{-1}(\mathbf{y}_m - \mathbf{h}_0))||_2^2 \tag{15}$$

$$\mathbf{C}_{\text{variance}} = \text{tr}((\mathbf{J}\mathbf{J}^T + r\mathbf{I})^{-1}\mathbf{J}\mathbf{M}^T\mathbf{M}\mathbf{J}^T(\mathbf{J}\mathbf{J}^T + r\mathbf{I})^{-1}) \tag{16}$$

Thus, mean-squared error is comprised of two components: $\mathbf{C}_{\text{bias}}$, the *bias*, represents the deterministic component of the error, and $\mathbf{C}_{\text{variance}}$, the *variance*, represents the stochastic component of the error, which originates from the amplification of the measurement noise. In the results that follow, we will be primarily interested in the bias that results from making incorrect assumptions about the breast background structure.

3. Results and Discussion

An MRI image of a healthy breast, shown in Fig. 1, was manually segmented into air, glandular, and adipose regions and interpolated onto a 2.5 mm uniform grid as shown in Fig. 2, part (a). The simulation results presented here were generated by a finite-difference forward model with 2 mm uniform grid spacing. A tumor of diameter 2 cm was simulated, centered at (x = 13 cm, y = 10 cm, z = 2.5 cm). The breast thickness is 7.5 cm, and we made use of simulated 70 MHz frequency-domain measurements, using 40 sources and 9 detectors, with a geometry as shown in Fig. 3. We assumed the following chromophore concentrations for the adipose and glandular regions, respectively: (20 μM HbO, 5 μM HbR, 30% H_2O 40% Lipid), and (22 μM HbO, 5.5 μM HbR, 40% H_2O 10% Lipid). The true chromophore distributions of breast tissue are yet to be determined experimentally, but we have chosen values to be consistent with published results (Shah et al. 2004). The following chromophore concentrations were simulated for the tumor, which has a greater blood volume and a lower oxygenation than the surrounding tissue (Fishkin et al. 1997): (40 μM HbO, 15 μM HbR, 20% H_2O 10% Lipid). The simulated tumor has a 50% perturbation in H_2O content, and has the same lipid concentration as the surrounding glandular tissue. Amplitude-dependent Gaussian noise with a variance of 1% was added to the measurements, and an identically distributed Gaussian phase uncertainty with a variance of 1° was assumed (Zhang et al. 2001).

We estimated background chromophore concentrations and reconstructed perturbations for four cases: true knowledge of the breast background structure, an assumed homogeneous background structure, a dilated glandular region, and an eroded glandular region. In the latter two cases, we increased and decreased the volume of the glandular part of the breast using erosion and dilation operators, as shown in Fig. 2, parts (b) and (c). The true volume

of the glandular tissue is 355 cm^3, and that of the adipose tissue is 817 cm^3. We dilated the glandular tissue to a volume of 544 cm^3, and eroded it to a volume of 239 cm^3.

The results of the background concentration estimation for the four cases is shown in Table 1. These results are graphically illustrated in Fig. 4. We note the fairly large variation in the estimates, particularly in the concentrations of H_2O and Lipids, for which there is a greater difference between the two regions. In part (b) of Fig. 4, the true tumor chromophore concentrations are also shown for the purpose of comparison.

In each of the above cases, we computed the Jacobian using these estimated background properties, and solved the linear inverse problem to reconstruct an image of the perturbation, making use of Eq. 10. The regularization parameter was chosen using the GCV criterion. The true solution, for the z = 2.5 cm slice is shown in Fig. 5, and the reconstructions, for the same slice, can be seen in Fig. 6. We note that an excellent spectroscopic reconstruction of a tumor in an inhomogeneous background can be obtained, provided that the background structure is known with a high degree of accuracy, as shown in part (a). On the other hand, the reconstruction assuming a homogeneous background is plagued by large image artifacts, shown in part (b). In comparing the dilated and eroded glandular cases, shown in (b) and (c), with the homogeneous case, we note that even imperfect prior information is useful in reducing image artifacts. In addition, the reconstructions for HbR and HbO in (c) and (d) are superior to the reconstruction for H_2O concentration, which is to be expected given the larger difference between the adipose and glandular tissue in their H_2O content. We believe that the superiority of reconstruction in the case of the assumed eroded glandular structure as compared to the case of the assumed dilated structure is not a general result, but rather is an effect introduced by particular cases studied in our simulations.

In order to further quantify the effect of imperfect background information on spectroscopic image reconstructions, we have computed the image reconstruction bias for each of the four cases, using Eq. 15, for perturbations in individual chromophores only. This bias is essentially computed by generating a linear reconstruction for each value of the regularization parameter, without any noise added to the measurements (zero-mean random noise manifests itself only in the variance). By using a perturbation in a single chromophore only, we can directly examine the reduction in bias as a function of the regularization parameter and also examine cross-talk, which is the leakage of a perturbation in one chromophore into the reconstruction for another chromophore.

Fig. 7 shows the per-voxel reconstruction bias for a 10 μM perturbation in HbO only as a function of the regularization parameter. The square root of the mean bias for voxels within and outside the tumor is shown using solid and dashed lines, respectively. Each quadrant shows the bias for all four chromophore reconstructions, for a given background structure assumption. In the case of perfect background structural information, shown in part (a), for the HbO reconstruction and voxels within the tumor we see the following behavior: for a large value of the regularization parameter, the bias is, as expected, 10 μM, meaning that

no perturbation is reconstructed where one is expected. The bias decreases to a minimum value as we reduce the level of regularization. After this point, discretization error in the iterative, numerical solution of the forward model tends to be amplified, resulting in image artifacts. Strictly speaking, this numerical quantization noise is deterministic, but different forward model implementations will produce quantitatively very different quantization noise realizations. Thus, our bias calculations for small values of the regularization parameter are particular to our finite-difference forward model implementation and grid resolution, although these results are likely to be qualitatively accurate for any numerically computed forward model. An additional reason for the bias tending to increase exponentially, even in the case of perfect background structural information, as we decrease the regularization parameter beyond a certain point, is that the actual measurements used in the inversion make use of a fully nonlinear model, while our inversion procedure assumes that a first-order linearization is accurate. Thus, this aspect of the model mismatch is amplified. The bias in the HbO reconstruction does not reach a minimum of zero because the regularization used here is not sufficient to overcome the inherent blurring in the forward model. Other regularization schemes may allow for a further reduction in bias.

For the HbO reconstruction, the value of the regularization parameter at which we see a minimum in the bias varies approximately two orders of magnitude, depending on the background structure assumption that is being made. Clearly the lowest achievable bias is attained when the background structure is known perfectly, shown in quadrant (a). We also see in this quadrant that even with perfect information, at the point that minizes bias in HbO there is still a small degree of spectroscopic cross-talk between the HbO reconstruction and the reconstructions for the other three chromophores. In quadrant (b), where we assume a homogeneous background, the minimum achievable bias is somewhat higher than in the case of perfect background information, as expected, and, at the value of the regularization parameter where the bias is minimized in HbO, we are beginning to see considerable bias in the H_2O reconstruction. In parts (c) and (d), in which we assume dilated and eroded glandular structures, respectively, it is somewhat surprising that the minimal achievable bias in HbO is not much different than in the case of perfect information, but, at this minimal point, we are beginning to see considerable bias in the reconstructions for the other three chromophores. In all four cases, the GCV algorithm returned a choice of regularization parameter between 0.1 and 1.0.

The square root of the mean bias for voxels outside of the tumor is shown using dashed lines, essentially quantifying the degree to which image artifacts are reconstructed by our inversion approach. Given our noise model and background assumptions, the H_2O reconstruction shows the greatest sensitivity to background modeling errors, as the value of the regularization parameter at which the image artifacts tend to increase exponentially is consistently higher than for the remaining chromophores. It is also interesting to observe that the value of the regularization parameter at which the bias seems to increase exponentially

differs for the bias within the tumor as compared to the bias outside the tumor. This indicates that when there is background modeling error, we have a trade-off between tumor reconstruction accuracy and background artifact suppression. We note the differences in regularization parameters at which point the artifacts tend to increase exponentially for the four background structure assumptions, which clearly show the greater presence of image artifacts as our knowledge of the background medium worsens. Parts (b), (c), and (d) show that a large bias in the estimate of background lipid concentration can be mitigated, to a certain extent, by the image reconstruction. It may be that more sophisticated approaches to the inverse problem solution can reduce the image artifact bias somewhat. For example, penalizing the image gradient rather than the image norm may tend to produce solutions which are more concentrated in a single region.

In order to analyze the minimal bias that is possible, both within and outside the tumor, we plot the reconstruction bias within the tumor vs. the bias for voxels outside the tumor in Fig. 8, over a wide range of regularization parameters. The optimal inversion scheme would intersect the origin, minimizing both the bias within the tumor and the image artifacts. For the reasons discussed above, even in the case of perfect background structural knowledge, we cannot achieve this goal, but our analysis shows the extent to which the best achievable reconstruction result varies as our knowledge of the background structure worsens. We note that assuming dilated or eroded background structures increases the within-tumor bias only modestly, given an optimal means for choosing the regularization parameter, but these assumptions increase the bias for voxels outside the tumor more substantially. As expected, the worst achievable result is attained when we assume a homogeneous background structure, in which case the minimum achievable bias within the tumor is significantly higher than for the other three cases, and the level of image artifacts is somewhat worse as well.

We have repeated the analysis above for perturbations in HbR, H_2O, and lipids, obtaining results that are qualitatively very similar to the case of an HbO perturbation. We have also computed the variance of the image reconstruction for the four cases of spatial prior information mentioned above, as we vary the regularization parameter. As expected from Eq. 16, in which the background structure estimate does not appear, the variance does not noticeably depend on the prior information used in the reconstruction.

4. Conclusion and Future Work

We have described a two-step algorithm for combining a high-resolution segmentation of the breast into distinct tissue types with a spectroscopic DOT reconstruction. In our approach, the background chromophore concentrations in the glandular and adipose regions are estimated using nonlinear Gauss-Newton iterations and the perturbation is estimated with a linearized spectroscopic reconstruction. If the segmentation is known with precision, we are able to both localize and characterize the tumor with very high accuracy.

Given that the true structure of the breast, as evidenced by MRI scans, is likely to be heterogeneous, we have explored the importance of this heterogeneity in linearized reconstructions. Specifically, we have reconstructed a perturbation when the breast background is assumed to be heterogeneous, though highly structured. We have examined the case where the breast is assumed to be homogeneous, and cases in which the assumed glandular tissue volume is "dilated" or "eroded" with respect to the true structure. In each of these cases, we have first estimated the background chromophore concentrations and then computed a perturbation assuming this estimate of the background optical properties. Our results clearly show that even incorrect knowledge of the background can be useful in localizing anomalies, but that the mismatch between our assumptions and reality can introduce severe bias in image reconstructions.

It is interesting to note that incorrect spatial prior structural information seems to have an asymmetric effect on the image reconstruction. This is evidenced by the fact that the minimum achievable bias within the simulated tumor increases more slowly than the minimum achievable bias outside of the tumor (i.e. the level of image artifacts) as the quality of our prior structural information worsens. It may be possible to use this tendency in image reconstruction algorithms, utilizing approaches specifically designed to designed to focus the solution of the inverse problem within a region of limited spatial support. Further research will also examine whether the prior information about the background structure can be applied in a probabilistic manner.

The analysis that we have conducted here gives us a framework for understanding the effect of our assumptions on reconstruction bias. As we improve our algorithms, the statistical approach shown here can quantify the reconstruction accuracy gains that are achievable, potentially justifying the additional computational cost. It is quite clear that, if there is significant optical heterogeneity within the breast, some sort of structural background prior information may be necessary if we are able to obtain quantatively accurate images using linearized methods. Future work will address whether this situation is improved if we make use of fully nonlinear optimization methods, and will also address the question of regularization parameter selection in the case of model mismatch. We also plan to examine how the results reported here generalize to the case where not only the constituent components of the breast are heterogeneous, but its scattering coefficient is spatially variant as well.

Acknowledgements

GB, ELM, and DHB acknowledge the support of CenSSIS, the Center for Subsurface Sensing and Imaging Systems, under the Engineering Research Centers program of the National Science Foundation (award number EEC-9986821). DAB, TC, QZ, and AL were supported by the National Institutes of Health.

References

Aronson, R. (1995), 'Boundary conditions for diffusion of light', *J. Opt. Soc. Am. A* **12**(11), 2532–2539.

Arridge, S. R. (1995), 'Photon measurement density functions. part 1: Analytical forms', *Applied Optics* **34**(31).

Arridge, S. R. (1999), 'Optical tomography in medical imaging', *Inverse Problems* **15**, R41–R93.

Banks, E., Reeves, G., Beral, V., Bull, D., Crossley, B., Simmonds, M., Hiltn, E., Bailey, S., Barrett, N., Briers, P., English, R., Jackson, A., Kutt, E., Lavelle, J., Rockall, L., Wallis, M. G., Wilson, M. & Patnick, J. (2004), 'Influence of personal chracteristics of individual women on sensitivity and specificity of mammography in the million women study: cohort study', *BMJ* **329**, 477–503.

Boas, D. A. (1996), Diffuse Photon Probes of Structural and Dynamical Properties of Turbid Media: Theory and Biomedical Applications, PhD thesis, University of Pennsylvania, Philadelphia, PA.

Boas, D. A., Brooks, D. H., Miller, E. L., Dimarzio, C. A., Kilmer, M., Gaudette, R. J. & Zhang, Q. (2001), 'Imaging the body with diffuse optical tomography', *IEEE Signal Processing Magazine* **18**(6), 57–75.

Boas, D. A., Gaudette, T. J. & Arridge, S. R. (2001), 'Simultaneous imaging and optode calibration with diffuse optical tomography', *Optics Express* **8**, 263–270.

Brooksby, B. A., Dehghani, H., Pogue, B. W. & Paulsen, K. D. (2003), 'Near-infrared (NIR) tomography breast image reconstruction with *a priori* structural information from MRI: algorithm development for reconstructing heterogeneities', *IEEE J. Sel. Top. Quant. Electr.* **9**(2), 199–209.

Cerussi, A. E., Berger, A. J., Bevilacqua, F., Shah, N., Jakubowski, D., Butler, J., Holcombe, R. F. & Tromberg, B. J. (2001), 'Sources of absorption and scattering contrast for near-infrared optical mammography', *Academic Radiology* **8**(3), 211–218.

Chance, B., Anday, E., Nioka, S., Zhou, S., Hong, L., Worden, K., Li, C., Ovetsky, M. T., Pidikiti, D. & Thomas, R. (1998), 'A novel method for fast imaging of brain function, non-invasively, with light.', *Optics Express* **2**(10), 411–423.

Cubbedu, R., D'Andrea, C., Pifferi, A., Taroni, P., Torricelli, A. & Valentini, G. (2000), 'Effects of the menstrual cycle on the red and near-infrared optical properties of the human breast', *Photochem. Photobiol.* **72**(3), 383–391.

Cubbedu, R., Pifferi, A., Taroni, P., Torricelli, A. & Valentini, G. (1999), 'Noninvasive absorption and scattering spectroscopy of bulk diffusive media: An application to the optical characterization of human breast', *Appl. Phys. Lett.* **74**(6), 874–876.

Dehghani, H., Pogue, B. W., Poplack, S. P. & Paulsen, K. D. (2003), 'Multiwavelength three-dimensional near-infrared tomography of the breast: initial simulation, phantom, and clinical results', *Applied Optics* **42**(1).

Durduran, T., Choe, R., Culver, J. P., Zubkov, L., Holboke, M. J., Giammarco, J. & Yodh, A. G. (2002), 'Bulk optical properties of healthy female breast tissue', *Phys. Med. Biol.* **47**, 2847–2861.

Elmore, J. G., Barton, M. B., Moceri, V. M., Polk, S., Arena, P. I. & Fletcher, S. W. (1998), 'Ten-year risk of false positive screening mammograms and clinical breast examinations', *N. Engl J. Med* **338**, 1089–1096.

Fishkin, J. B., Coquoz, O., Anderson, E. R., Brenner, M. & Tromberg, B. J. (1997), 'Frequency-domain photon migration measurements of normal and malignant tissue optical properties in a human subject', *Applied Optics* **36**(1), 10–20.

Fletcher, S. W. & Elmore, J. G. (2003), 'Mammographic screening for breast cancer', *New England Journal of Medicine* **348**, 1672–1680.

Franceschini, M. A., Moesta, K. T., Fantini, S., Gaida, G., Gratton, E., Jess, H., Mantulin, W. W., Seeber, M., Schlag, P. M. & Kaschke, M. (1997), 'Frequency-domain techniques enhance optical mammography: Initial clinical results', *Proc. Natl. Acad. Sci. USA* **94**, 6468–6473.

Franceschini, M. A., Toronov, V., Filiaci, M., Gratton, E. & Fantini, S. (2000), 'On-line optical imaging of

the human brain with 160-ms temporal resolution.', *Optics Express* **6**(3), 49–57.

Gaudette, R., Brooks, D., Dimarzio, C. & Boas, D. (1999), 'Multi-wavelength diffuse optical tomography: Experimental results', *Proceeding of the Conference on Laseres and Electro-Optics* pp. 253–254.

Golub, G. H., Heath, M. H. & Wahba, G. (1979), 'Generalized cross-validation as a method for choosing a good ridge parameter', *Technometrics* **21**(2), 215–222.

Golub, G. H. & von Matt, U. (1997), 'Generalized cross-validation for large-scale problems', *Journal of Computational and Graphical Statistics* **6**(1), 1–34.

Grosenick, D., Wabnitz, H., Rinneberg, H. H., Moesta, K. T. & Schlag, P. M. (1999), 'Development of a time-resolved optical mammograph and first in-vivo applications', *Appl. Opt.* **38**(13), 2927–2943.

Guven, M., Yazici, B., Intes, X. & Chance, B. (2005), 'Diffuse optical tomography with *a priori* anatomical information', *Phys. Med. Biol.* **50**, 2837–2858.

Haskell, R. C., Svaasand, L. O., Tsay, T. T., Feng, T., McAdams, M. S. & Tromberg, B. J. (1994), 'Boundary conditions for the diffusion equation in radiative transfer', *J. Opt. Soc. Am. A* **11**(10), 2727–2741.

Hebden, J. C., Gibson, A., Yusof, R., Everdell, N., Hillman, E. M. C., Delpy, D. T., Arridge, S. R., Austin, T. & Meek, J. H. (2002), 'Three-dimensional optical tomography of the premature infant brain', *Phys. Med. Biol.* **47**, 4155–4166.

Hero, A. O., Piramuthu, R., Fessler, J. A. & Titus, S. R. (1999), 'Minimax emission computed tomography using high-resolution anatomical information and B-spline models', *IEEE Transactions on Information Theory* **45**(3), 920–938.

Hillman, E. M. C. (2002), Experimental and theoretical investigation of near-infrared tomographic imaging methods and clinical investigations, PhD thesis, University of London, London, UK.

Huang, M., Xie, T., Chen, N. G. & Zhu, Q. (2003), 'Simultaneous reconstruction of absorption and scattering maps with ultrasound localization: feasibility study using transmission geometry', *Applied Optics* **42**(19), 4102–4114.

Intes, X., Maloux, C., Guven, M., Yazici, B. & Chance, B. (2004), 'Diffuse optical tomography with physiological and spatial *a priori* constraints', *Phys. Med. Biol.* **49**, N155–N163.

Jiang, H. B., Paulsen, K. D., Osterberg, U. L. & Patterson, M. S. (1997), 'Frequency-domain optical image reconstruction in turbid media: an experimental study of single-target detectability', *Applied Optics* **36**(1), 52–63.

Jiang, H., Paulsen, K. D., Osterberg, U. L., Pogue, B. W. & Patterson, M. S. (1996), 'Optical image reconstruction using frequency-domain data: simulations and experiments', *J. Opt. Soc. Am. A* **13**(2), 253–266.

Li, A., Boverman, G., Zhang, Y., Brooks, D., Zhang, Q., Hillman, E. M. C. & Boas, D. A. (2005), 'An optimal linear inverse solution given multiple priors in diffuse optical tomography', *Accepted for publication, Applied Optics* .

Li, A., Miller, E. L., Kilmer, M. E., Brukilacchio, T. J., Chaves, T., Stott, J., Zhang, Q., Wu, T., Chorlton, M., Moore, R. H., Kopans, D. B. & Boas, D. A. (2003), 'Tomographical optical breast imaging guided by three-dimensional mammography', *Applied Optics-OT* **42**, 5181–5190.

Li, A., Zhang, Q., Culver, J. P., Miller, E. L. & Boas, D. A. (2004), 'Reconstructing chromosphere concentration images directly by continuous-wave diffuse optical tomography', *Optics Letters* **29**(3), 256–258.

McBride, T. O., Pogue, B. W., Gerety, E. D., Poplack, S. R., Osterberg, U. L. & Paulsen, K. D. (1999), 'Spectroscopic diffuse optical tomography for the quantitative assessment of hemoglobin concentration and oxygen saturation in breast tissue', *Appl. Opt.* **38**(25), 5480–5490.

Milstein, A. B., Oh, S., Reynolds, J. S., Webb, K. J. & Bouman, C. A. (2002), 'Three-dimensional Bayesian optical diffusion tomography with experimental data', *Optics Letters* **27**(2), 95–97.

Oh, S., Milstein, A. B., Millane, R. P., Bouman, C. A. & Webb, K. J. (2002), 'Source-detector calibration in three-dimensional bayesian optical diffusion tomography', *J. Opt. Soc. Am. A* **19**(10), 1983–1993.

Paige, C. C. & Saunders, M. A. (1982), 'LSQR: An algorithm for sparse linear equations and sparse least squares', *ACM Transactions on Mathematical Software* **8**, 43–71.

Pogue, B. W. & Paulsen, K. D. (1998), 'High-resolution near-infrared tomographic imaging simulations of the rat cranium by the use of *a priori* magnetic resonance structural information', *Optics Letters* **23**(21), 1716–1718.

Pogue, B. W., Poplack, S. P., McBride, T. O., Wells, W. A., Osterman, K. S., Osterberg, U. L. & Paulsen, K. D. (2001), 'Quantitative hemoglobin tomography with diffuse near-infrared spectroscopy: pilot results in the breast', *Radiology* **218**(1), 261–266.

Shah, N., Cerussi, A. E., Jakubowski, D., Hsiang, D., Butler, J. & Tromberg, B. J. (2004), 'Spatial variations in optical and physiological properties of healthy breast tissue', *Journal of Biomedical Optics* **9**(3), 534–540.

Shah, N., Cerussi, A., Eker, C., Espinoza, J., Butler, J., Fishkin, J., Hornung, R. & Tromberg, B. (2001), 'Noninvasive functional optical spectroscopy of human breast tissue', *Proceedings of the National Academy of Science, USA* **98**(8), 4420–4425.

Srinivasan, S., Pogue, B. W., Jiang, S., Dehghani, H., Kogel, C., Soho, S., Gibson, J. J., Tosteson, T. D., Poplack, S. P. & Paulsen, K. D. (2003), 'Interpreting hemogobin and water concentration, oxygen saturation, and scattering measured *in vivo* by near-infrared breast tomography', *Proc. Natl. Acad. Sci.* **100**(21), 12349–12354.

Vernieri, F., Rosato, N., Pauri, F., Tibuzzi, F., Passarelli, F. & Rossini, P. M. (1999), 'Near infrared spectroscopy and transcranial doppler in monohemispheric stroke', *Eur. Neurol.* **41**, 159–62.

Zhang, Q., Brukilacchio, T. J., Gaudett, T., Wang, L., Li, A. & Boas, D. A. (2001), Experimental comparison of using continuous-wave and frequency-domain diffuse optical imaging systems to detect heterogeneities, *in* B. Chance, R. R. Alfano, B. J. Tromberg, M. Tamura & E. M. Sevick-Muraca, eds, 'Optical Tomography and Spectroscopy of Tissue IV', SPIE, Bellingham, WA, pp. 219–238.

Table 1. Estimates of background chromophore concentrations

	Adipose region			
	HbO (μM)	HbR (μM)	Water (%)	Lipid (%)
True concentrations	20	5	30	40
Homogeneous assumed	21.09	5.29	36.21	22.63
Dilated glandular assumed	19.18	4.81	27.07	49.96
Eroded glandular assumed	20.20	5.05	31.22	36.30
	Glandular region			
	HbO (μM)	HbR (μM)	Water (%)	Lipid (%)
True concentrations	22	5.5	40	10
Homogeneous assumed	21.09	5.29	36.21	22.63
Dilated glandular assumed	21.72	5.43	38.14	15.23
Eroded glandular assumed	22.47	5.64	42.13	4.02

List of Figure Captions

Fig. 1. Slices of a fat-suppressed MRI scan at several depths. (a) z = 1.2 cm (b) z = 2.4 cm (c) z = 4.0 cm

Fig. 2. Breast geometries used in the simulation. (a) Geometry derived from manually-segmented MRI Image (b) Geometry with a dilated glandular region (c) Geometry with an eroded glandular region

Fig. 3 Source and detector configurations used in the simulations. (a) Source configuration (b) Detector configuration

Fig. 4 Estimated background chromophore concentrations (a) Adipose tissue (b) Glandular tissue, with the true chromophore concentrations of the tumor shown for the purpose of comparison.

Fig. 5 True solution for absorption concentrations

Fig. 6 Linear reconstructions of chromophore concentrations given a number of assumptions about the breast background. (a) Reconstruction assuming accurate knowledge of background structure. (b) Reconstruction assuming a homogeneous background. (c) Reconstruction assuming a dilated glandular region. (d) Reconstruction assuming an eroded glandular region.

Fig. 7 Reconstruction bias for an HbO-only perturbation as a function of the regularization parameter. (a) Reconstructions bias when the background is known exactly. (b) Bias when a homogeneous background is assumed. (c) Bias assuming a dilated glandular region. (d) Bias assuming an eroded glandular region. Note that the bias is given in the units that are natural for each chromophore (i.e. μM for HbO and HbR and percentage for H_2O and Lipids). The horizontal axis shows the logarithm, base 10, of the regularization parameter.

Fig. 8 Within-Tumor bias vs. outside-tumor bias, for a perturbation in HbO only, for each of the background structure assumptions, over a wide range of regularization parameters.

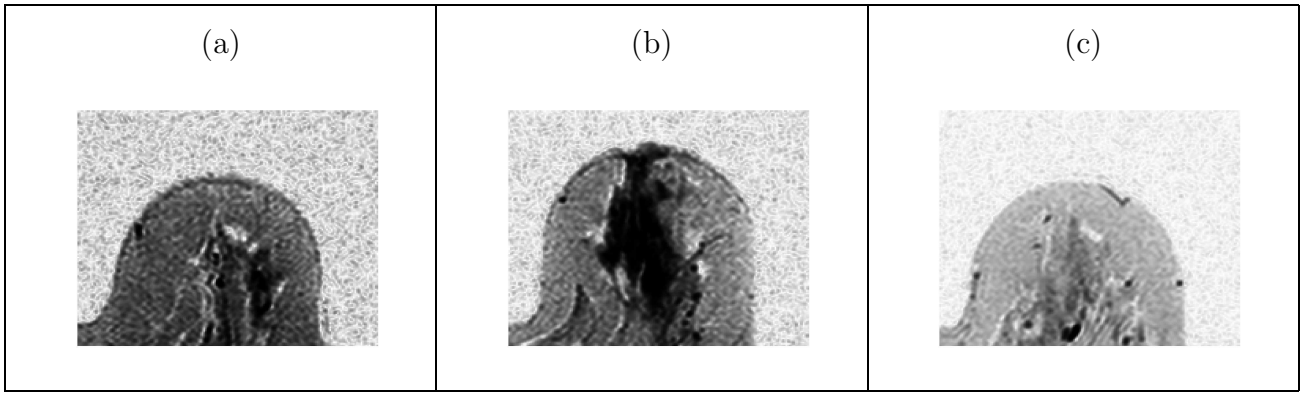

Figure 1. Slices of a fat-suppressed MRI scan at several depths. (a) z = 1.2 cm (b) z = 2.4 cm (c) z = 4.0 cm

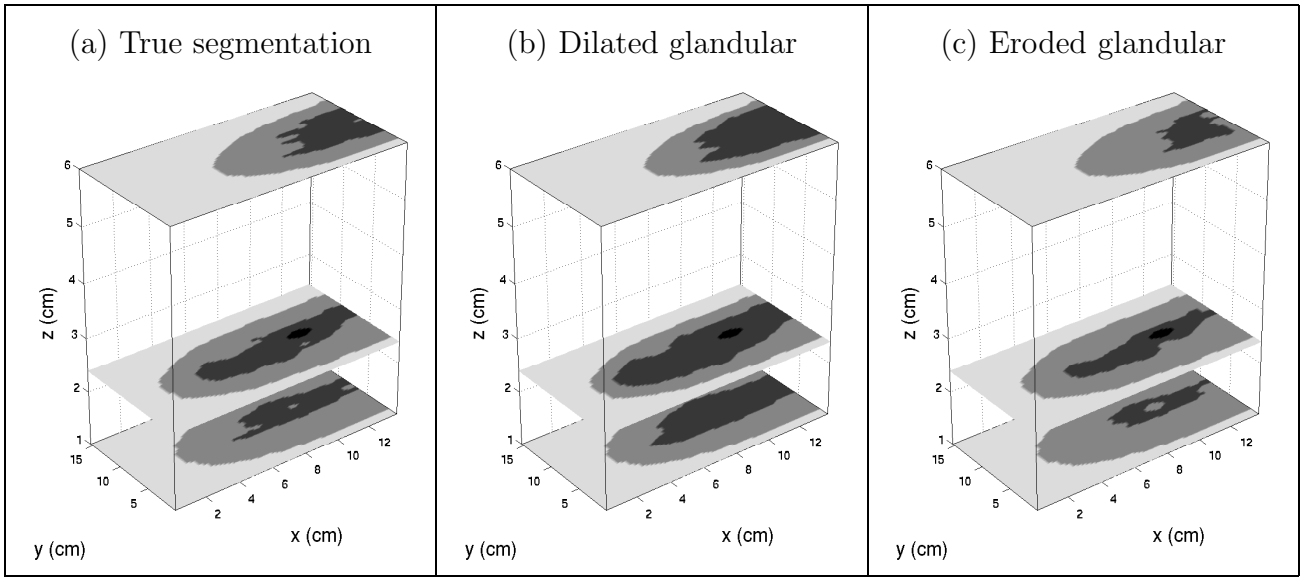

Figure 2. Breast geometries used in the simulation. (a) Geometry derived from manually-segmented MRI Image (b) Geometry with a dilated glandular region (c) Geometry with an eroded glandular region

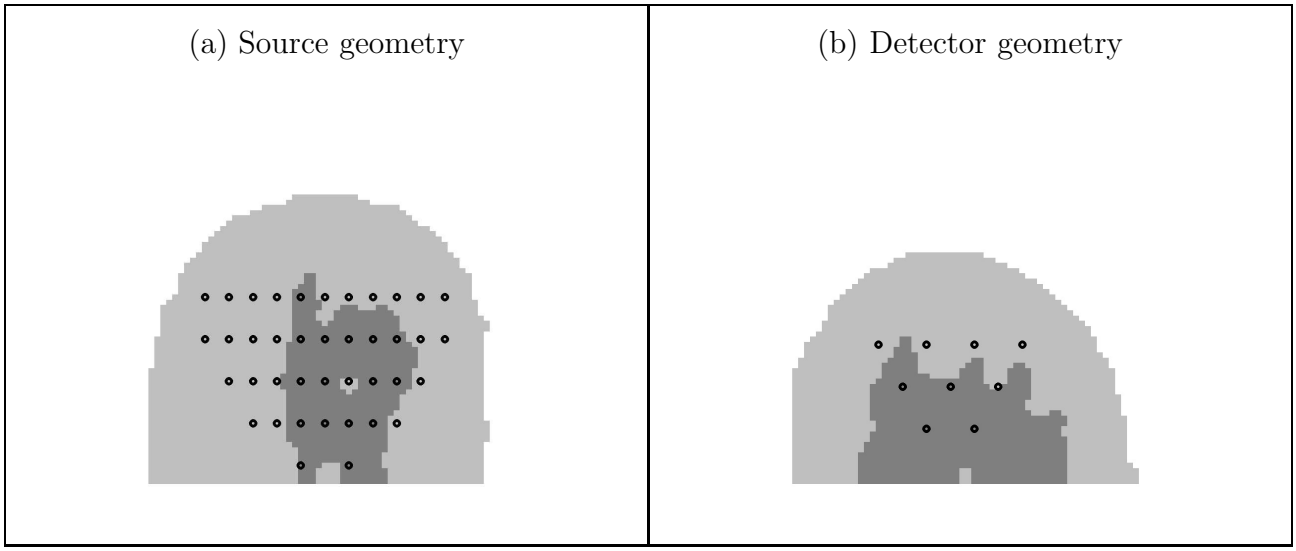

Figure 3. Source and detector configurations used in the simulations. (a) Source configuration (b) Detector configuration

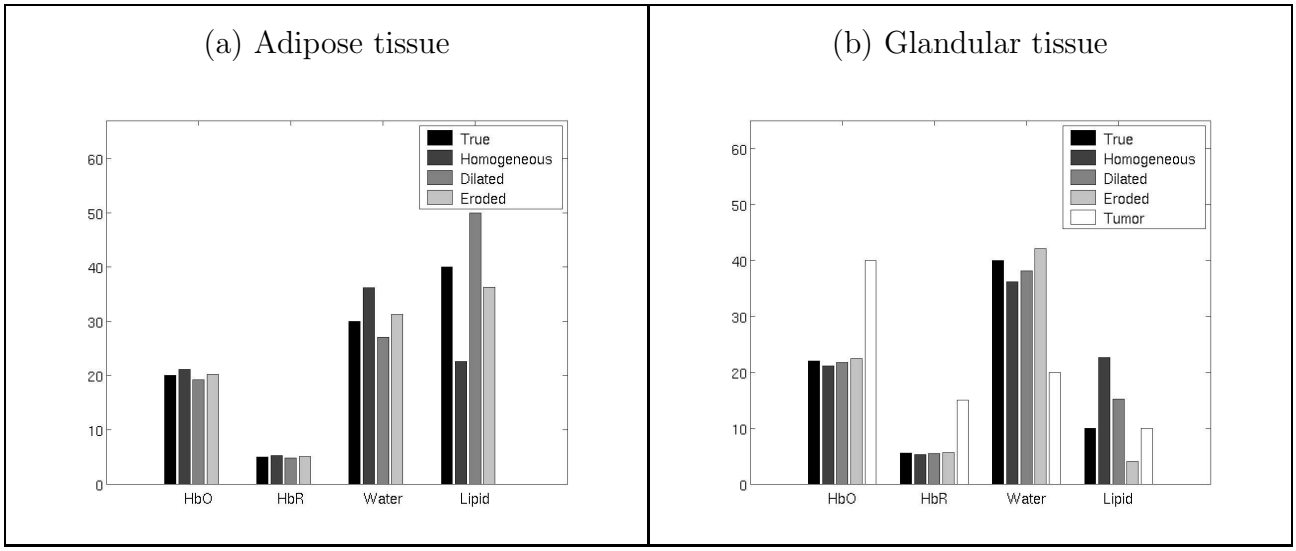

Figure 4. Estimated background chromophore concentrations (a) Adipose tissue (b) Glandular tissue, with the true chromophore concentrations of the tumor shown for the purpose of comparison.

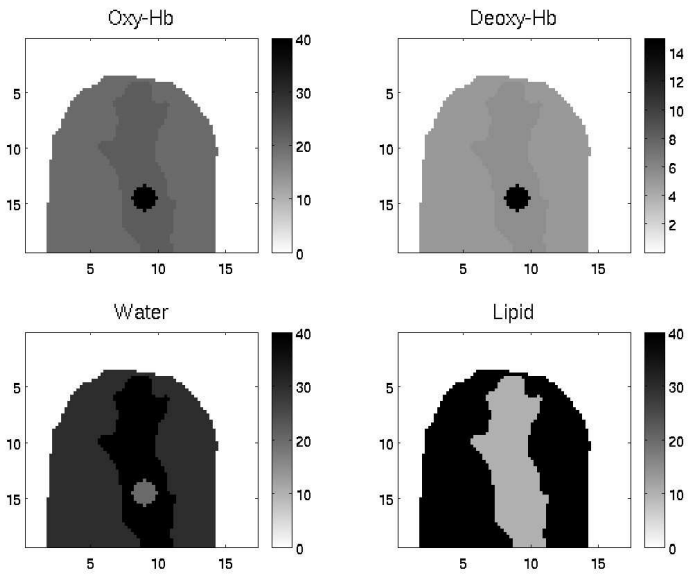

Figure 5. True solution for absorption concentrations

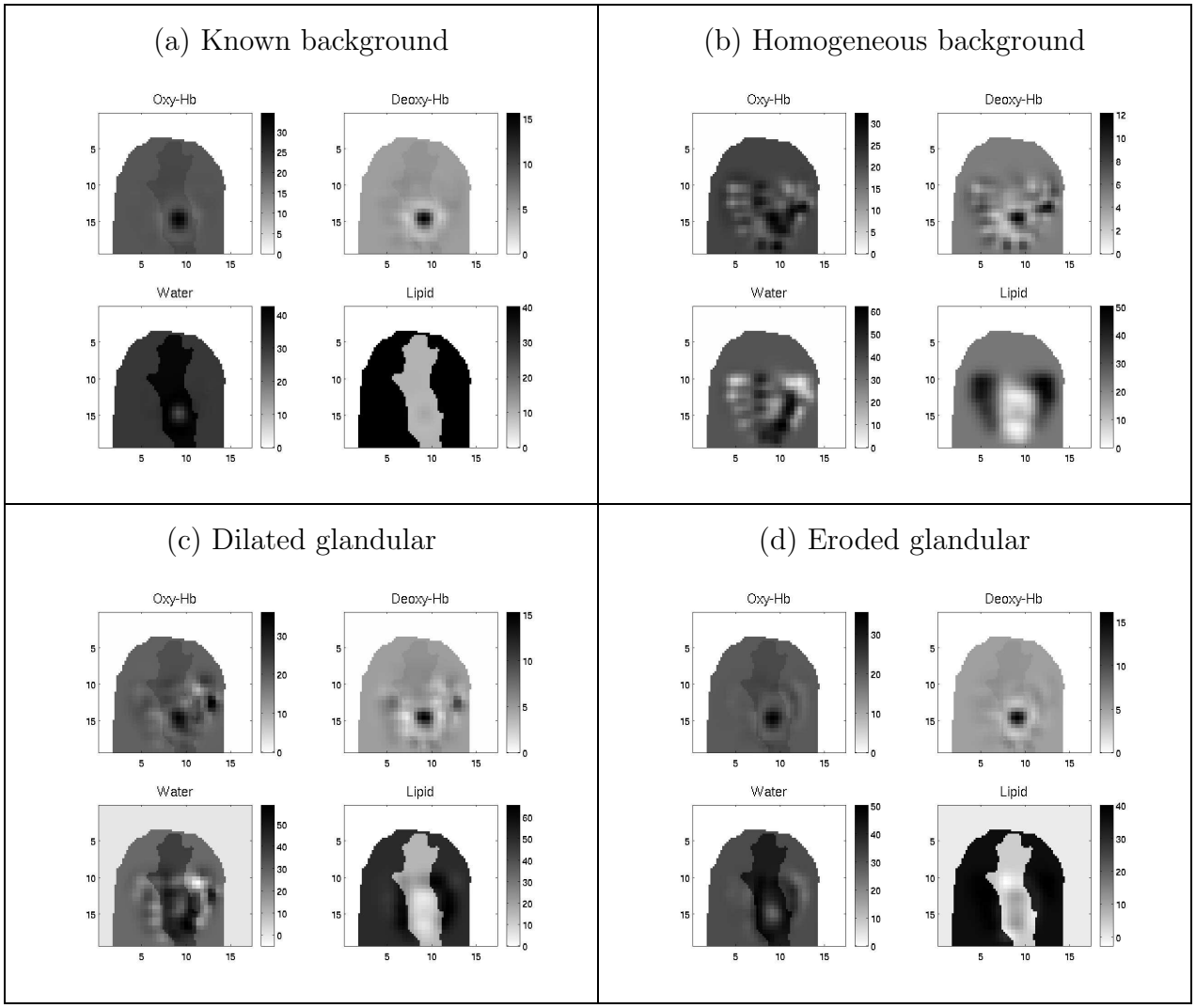

Figure 6. Linear reconstructions of chromophore concentrations given a number of assumptions about the breast background. (a) Reconstruction assuming accurate knowledge of background structure. (b) Reconstruction assuming a homogeneous background. (c) Reconstruction assuming a dilated glandular region. (d) Reconstruction assuming an eroded glandular region.

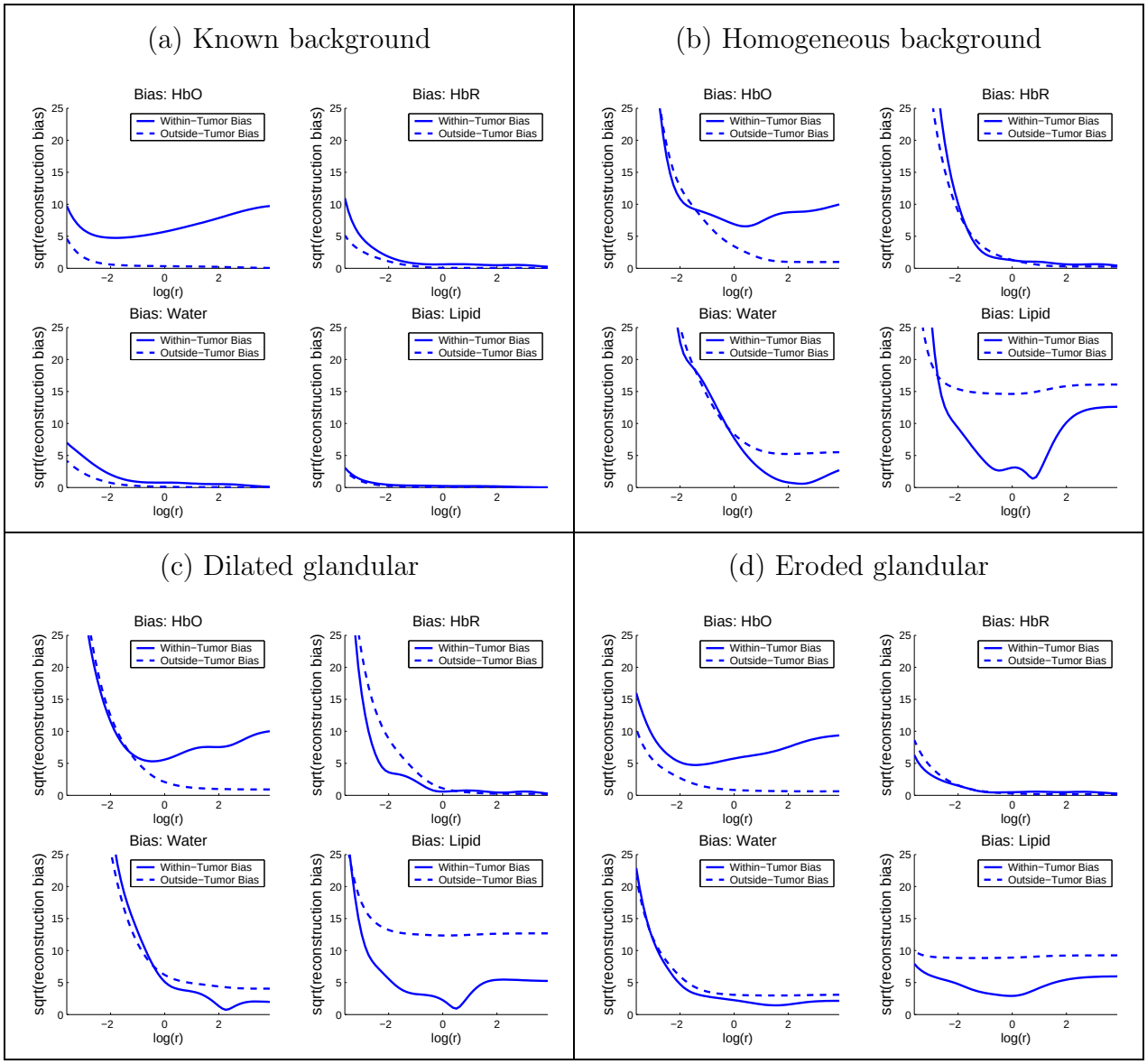

Figure 7. Reconstruction bias for an HbO-only perturbation as a function of the regularization parameter. (a) Reconstructions bias when the background is known exactly. (b) Bias when a homogeneous background is assumed. (c) Bias assuming a dilated glandular region. (d) Bias assuming an eroded glandular region. Note that the bias is given in the units that are natural for each chromophore (i.e. μM for HbO and HbR and percentage for H_2O and Lipids). The horizontal axis shows the logarithm, base 10, of the regularization parameter.

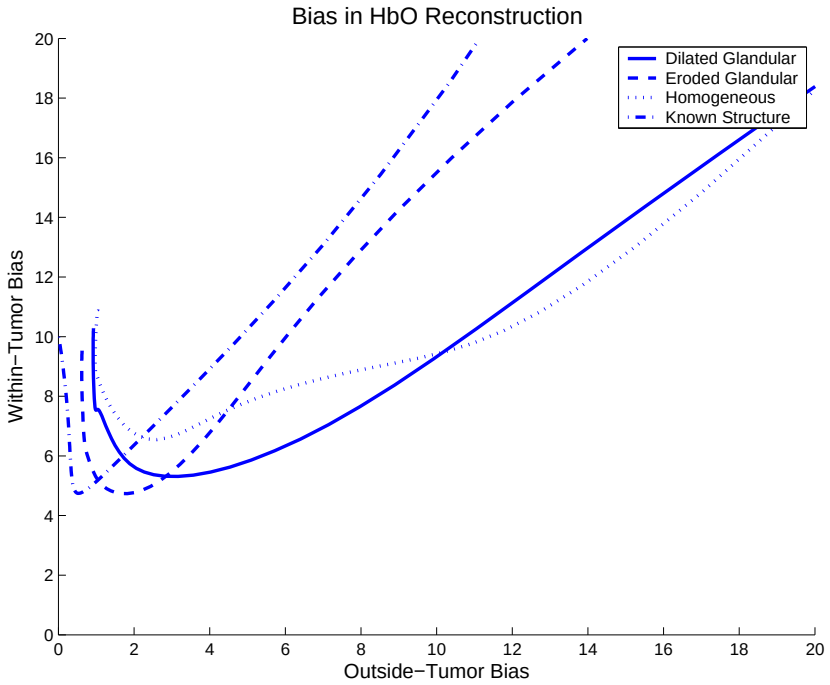

Figure 8. Within-Tumor bias vs. outside-tumor bias, for a perturbation in HbO only, for each of the background structure assumptions, over a wide range of regularization parameters.